Thermodynamic Instability of Human λ6 Light Chains: Correlation with Fibrillogenicity†

Jonathan Wall,*,‡ Maria Schell,‡ Charles Murphy,‡ Rudi Hrncic,‡ Fred J. Stevens,§ and Alan Solomon‡

Human Immunology and Cancer Program, University of Tennessee Graduate School of Medicine at Knoxville, 1924 Alcoa Highway, Knoxville, Tennessee 37920-6999, and Center for Mechanistic Biology and Biotechnology, Argonne National Laboratory, Argonne, Illinois 60439

Received May 17, 1999; Revised Manuscript Received August 17, 1999

ABSTRACT: Certain types of human light chains have the propensity to deposit pathologically as amyloid fibrils as evidenced by the preferential association of monoclonal λ6 proteins with AL amyloidosis. However, the molecular features that render such proteins amyloidogenic have not been elucidated. Based upon the demonstrated relationship between the thermodynamic stability of light chains and their propensity to aggregate in vitro, we have initiated studies where the thermodynamic properties and fibrillogenic potential of two recombinant (r) $V_\lambda 6$ molecules were compared. The first protein was generated from cDNA cloned from marrow-derived plasma cells from a patient (Wil) who had AL amyloidosis and renal amyloid deposits; the second was from a patient (Jto) with multiple myeloma in whom the λ6 protein was deposited not as amyloid but in the form of renal tubular casts. The thermodynamic stabilities of $rV_\lambda 6$Wil and -Jto were determined from chaotropic and thermal denaturation studies. Based upon the ΔG_{H2O}, ΔH, $\Delta G_{25\ °C}$, T_m, and C_m values, the $rV_\lambda 6$Wil was less stable than its nonamyloidogenic counterpart, $rV_\lambda 6$Jto. Measurement of fibril formation using a novel in vitro fibril forming assay demonstrated that although both $rV_\lambda 6$ proteins formed fibrils in vitro, Wil had a shorter lag time and exhibited faster kinetics under physiologic conditions. Comparative amino acid sequence analyses of these two components and other λ6 amyloid-associated light chains revealed that the Jto protein had certain primary structural features that we posit contributed to its increased stability and thus rendered this protein nonamyloidogenic. Our studies provide the first evidence that stabilizing interactions within the V_L domain can influence the kinetics of light chain fibrillogenicity.

The aggregation of normally soluble proteins into fibrils is the pathologic mechanism underlying a family of disease states known as the amyloidoses (*1*). To date, approximately 18 different amyloid-precursor proteins have been identified. These molecules are involved in diseases such as Alzheimer's disease, type II diabetes, familial polyneuropathy, and primary, i.e., light-chain associated (AL),[1] amyloidosis (*2*). Irrespective of the type of precursor protein, all types of amyloid have a similar ultrastructure; namely, they consist of 8−10 nm diameter fibrils of indeterminate length in which the proteins adopt a cross-β-sheet conformation with strands oriented roughly perpendicular to the long axis of the fibril. This feature suggests a common mechanism underlying fibrillogenesis, which may be akin to crystallization (*3*).

AL amyloidosis represents a plasma cell dyscrasia (*4*) in which monoclonal immunoglobulin (Ig) light chains (i.e., Bence Jones proteins) are deposited as fibrils in vital organs, causing dysfunction. These proteins can also deposit as amorphous casts, basement membrane precipitates, or intracellular crystals as found in patients with myeloma (cast) nephropathy, light chain deposition disease (LCDD), and adult (acquired) Fanconi syndrome, respectively (*5*, *6*), or in other cases are apparently nontoxic. Based on experimental data, it has become increasingly evident that certain primary structural features of light chains enhance or diminish the pathologic potential of these proteins. Comparative amino acid sequence analyses of pathologic and nonpathologic proteins have indicated that certain amino acid substitutions at particular sites within the light chain variable domain (V_L) may potentiate fibril formation. Using recombinant (r) V_L fragments, Hurle et al. (*7*) have shown that certain amino acid substitutions destabilized these molecules, resulting in an increased propensity to self-aggregate. Additionally, a correlation between the thermodynamic stability of Bence Jones proteins and their behavior in vivo has been found (*8*). In particular, proteins obtained from patients with AL were less stable than clinically nontoxic components or those associated with cast nephropathy, or LCDD (*8*, *9*).

It is noteworthy that in patients with myeloma (cast) nephropathy and LCDD, κ-type monoclonal Igs predominate. This contrasts to the prevalence of λ components in AL. Most remarkable has been the finding that λ proteins of one particular V_λ subgroup ($V_\lambda 6$) are typically associated with

† This work was supported by USPHS Grant CA10056 from the National Cancer Institute. A.S. is an American Cancer Society Clinical Research Professor.

* To whom correspondence should be addressed. Telephone: (423) 544 9165. Fax: (423) 544 6865. E-mail: jwall@mc.utmck.edu.

‡ University of Tennessee Graduate School of Medicine at Knoxville.

§ Argonne National Laboratory.

[1] Abbreviations: ThT, thioflavin T; V_L, light chain variable domain; GdHCl, guanidine hydrochloride; r, recombinant; AL, light chain associated (primary) amyloidosis.

10.1021/bi991131j CCC: $18.00
Published on Web 09/30/1999

this process. Heretofore, the primary structural features that render λ6 light chains amyloidogenic have not been elucidated. Our recent discovery of a patient (Jto) with multiple myeloma and a λ6 Bence Jones protein that formed renal tubular casts rather than amyloid provided us a unique opportunity to evaluate intrinsic factors that effect light chain pathogenicity. We have prepared $rV_\lambda6$ components based upon the sequences of the V_L proteins Jto and that of an amyloid-associated λ6 protein, Wil. Our studies of these two components revealed a striking difference in the thermodynamic properties and that stabilizing interactions within the V_L can influence the potential of light chains to form amyloid.

MATERIALS AND METHODS

Patients Jto and Wil. Patient Jto was a 60-year-old male with typical features of multiple myeloma, including osteolytic skeletal lesions and biopsy-proven tubular cast nephropathy that eventuated in renal failure. An IgGλ6 and λ6 Bence Jones protein were detected in the urine and serum, respectively. There were ~50% monotypic λ6-containing plasma cells in the bone marrow. The λ6 protein composition of renal tubular casts was demonstrated immunohistochemically. No amyloid deposits could be detected in biopsy specimens of kidney, bone marrow, and multiple samples of subcutaneous fat aspirates.

Patient Wil was a 64-year-old female in whom a diagnosis of AL amyloidosis was established on the basis of typical clinicopathologic and laboratory criteria. Immunofixation electrophoresis of serum and urine specimens disclosed the presence of a λ-type IgG and Bence Jones protein, respectively. Bone marrow examination revealed ~9% λ^+ plasma cells. Amyloid deposition was evidenced in a Congo red-stained biopsy specimen of kidney and was shown in immunofluorescence studies to be λ light chain related. Immunohistochemical and serologic analyses using anti-human V_λ subgroup-specific monoclonal antibodies (*10*) revealed the $V_\lambda6$ nature of the serum and urine monoclonal components, plasma cell cytoplasmic immunoglobulins, and amyloid.

Isolation and Cloning of cDNA from Jto and Wil. An enriched population of bone marrow-derived plasma cells was obtained by separation on a 50% Percoll gradient. These cells were used to isolate total RNA for RT-PCR by methods described previously (*11*). For the isolation of the $V_\lambda6$Jto cDNA fragment, 1 μg of total RNA was used for first-strand cDNA synthesis, and single-strand cDNA was amplified using the $V_\lambda6$-specific VL6-3 upstream and C_λ universal downstream primers (*12*). The amplified germline DNA (632 bp) and cDNA (537 bp) fragments were cloned into the pNoTA/T7 vector using the Prime PCR Cloner System (5 Prime-3 Prime Inc., Boulder, CO), and the nucleotide sequence of the resulting clones, designated JTO-G and JTO-C respectively, was determined by the dideoxynucleotide method (*13*).

Cloning of JTO and SW cDNAs into pET-27b(+) Vector. Primer pairs JTVL6 For/JTVL6 Rev and SWVL6 For/SWVL6 Rev were designed to amplify specifically a 350 bp fragment corresponding to the region between FR1 and FR4 using the clones JTO-C and LV6SW-C as DNA templates (*11*). The PCR products were purified, digested with *Eco*RI and *Msc*I restriction enzymes (New England Biolabs, Inc., Beverly, MA), and cloned into the *Eco*RI/*Msc*I-digested pET-27b(+) vector (Novagen, Inc., Madison, WI). The resulting clones, designated pET-JTO and pET-SW, were transformed into *E. coli* BL21(DE3)-competent cells (Novagen, Inc.), and their sequence was determined.

Expression of pET-JTO and pET-SW in E. coli. Proteins were expressed in *E. coli* under the control of the T7 *lac* promoter with a *pel* B leader sequence directing export to the periplasm of the cell. Transformed BL21(DE3) cells were grown overnight at 37 °C in 25 mL of LB culture media (*14*) containing 30 μg/mL kanamycin sulfate [LB/Kan (Sigma Chemicals)], with agitation at 225 rpm in an orbital shaker. A 1.2 L volume of LB/Kan culture media was inoculated with the overnight starter culture and grown to an A_{600} of ~0.6−0.8. The cells were induced by the addition of isopropyl β-D-thiogalactopyranoside to a final concentration of 1 mM. After 4 h, the cells were recovered by centrifugation, frozen, and processed as described below. To obtain $rV_\lambda6$Wil in a soluble form that could be isolated from the periplasm, it was necessary to change the temperature and agitation conditions to 30 °C and 125 rpm, respectively.

Protein Purification. Protein purification was performed using a modification of the manufacturer's protocol (Novagen, Inc.). Cell pellets from the 1.2 L culture were resuspended in 0.4 volume (480 mL) of 20% sucrose, 30 mM Tris-HCl, pH 8.0, buffer, EDTA (pH 8.0) was added to a final concentration of 1 mM, and the tubes were shaken at room temperature for 10 min. The cells were centrifuged at 4 °C for 10 min at 10 000 rpm, resuspended in 0.4 volume (480 mL) of ice-cold 5 mM $MgSO_4$ buffer, shaken on ice for 15 min, and centrifuged as above. Amberlite XAD-7 (Sigma Chemicals) was added to the supernatant at 10 wt %/v, and the mixture was stirred at room temperature for 2 h. Half of the liquid was decanted and the protein eluted from the Amberlite by the addition of 240 mL of 50% acetonitrile/0.1% TFA. After being stirred for 15 min, the protein-containing solution was dialyzed against water and lyophilized. The protein was then subjected to reverse-phase HPLC (ABI, Foster City, CA) and analyzed for purity by HPLC and SDS−PAGE. The ratios of monomeric and dimeric forms of $rV_\lambda6$Wil and -Jto in solution were determined by size-exclusion chromatography; proteins were suspended in phosphate-buffered saline (150 mM NaCl, 10 mM Na_2HPO_4, 10 mM NaH_2PO_4, pH 7.5; PBS) at 70 μg/mL and passed through a 0.2 μm pore-size filter (Acrodisc). The proteins were analyzed using a BioLogic (BioRad, Hercules, CA) medium-pressure chromatography system equipped with a Bio-Sil SEC 250 column (BioRad); PBS was used as the mobile phase with a flow rate of 0.9 mL/min. A total of 500 μL of protein solution was injected onto the column; eluted proteins were detected by their absorbance at 280 nm. The column was normalized using known protein standards (BioRad). The molecular weight of each $V_\lambda6$ component was determined by analyzing the elution chromatogram with a peak-fitting program (Grams/32, Galactic Industries Corp., Salem, NH).

Protein Preparation for Spectrofluorometric Analyses. Solutions of $rV_\lambda6$Wil and -Jto were prepared from stocks by dilution into PBS followed by filtration through a 0.2 μm pore-sized filter (Acrodisc) to remove preformed aggregates. The final protein concentration was then determined

spectrophotometrically using molar extinction coefficients of 12 210 and 13 490 for rV$_\lambda$6Wil and -Jto, respectively, as calculated from the amino acid sequence using the program PEPTIDESORT. Protein samples were subjected to filtration and concentration determination prior to each denaturation and fibrillogenesis experiment.

GdHCl Denaturation. Thermodynamic stabilities of rV$_\lambda$-6Wil and -Jto were determined by denaturation in guanidine hydrochloride (GdHCl) as follows: Protein solutions (20 μg/mL) were prepared in increasing concentrations of GdHCl up to 4 M buffered with 10 mM sodium phosphate, pH 7.5. The samples were incubated overnight at 25 °C. The extent of denaturation was determined by measuring the increase in tryptophan (Trp35) fluorescence. Samples were placed in a 600 μL volume quartz cuvette (Spectrocell Corp., Orland, PA), and the fluorescence intensity was measured using an SLM Aminco Bowman (Series II) spectrofluorometer. Excitation and emission wavelengths were 295 and 350 nm, respectively. Corresponding slit widths of 4 and 8 nm were used, and the photomultiplier (PMT) voltage was set to 800 V. Data were collected in duplicate for each GdHCl concentration and analyzed according to Santoro and Bolen (*15*) as follows. Equation 1 was applied to the data using the nonlinear, least-squares fitting program ULTRAFIT (Biosoft, U.K.):

$$F_{\mathrm{Trp}} = \frac{[(y_n + m_n[\mathrm{D}]) + (y_d + m_d[\mathrm{D}])\exp -(\Delta G^\circ_{\mathrm{H_2O}}/RT + m_g[\mathrm{D}]/RT)]}{[1 + \exp -(\Delta G^\circ_{\mathrm{H_2O}}/RT + m_g[\mathrm{D}]/RT)]} \quad (1)$$

where y_x and m_x are the *y*-intercept and gradient of the linear equations for the native ($_n$) and denatured ($_d$) forms of the protein; [D] is the GdHCl concentration; $\Delta G^\circ_{\mathrm{H_2O}}$ is the free energy change for the conversion of the native to the denatured state in the absence of denaturant; m_g is the gradient of the linear, transition region and reflects the cooperativity of the reaction; *R* and *T* are the gas constant and absolute temperature, respectively. The GdHCl concentration at the midpoint of the transition (C_m) was calculated by a least-squares fit of the data to an exponential sigmoid.

Thermal Denaturation. Proteins rV$_\lambda$6Wil and -Jto were suspended to a final concentration of 70 μg/mL in a 2.5 mL volume of PBS. The samples were placed into a 3 mL volume quartz cuvette, and the Trp35 fluorescence intensity was measured as described above; however, for these studies, the PMT voltage was lowered to 750 V, and a micro-stir bar was used at very low speed to equilibrate the solution temperature. Data points were collected every second. The samples were heated using a circulating water bath attached to the cuvette holder. The water bath temperature was ramped from the initial 25 °C to 60 °C in a single step, resulting in a temperature increase rate of 0.04 °C s^{-1}. The solution temperature was measured directly using a k-type thermoprobe inserted into the cuvette; these data were imported directly into the spectrofluorometer in real-time via an analogue input port. A correction factor (slope) was applied to the thermoprobe signal, and the data were stored in an ASCII format. This system allowed data values for the temperature (abscissa) and the fluorescence intensity (ordinate) to be collected every second and plotted directly against each other. There were no visible aggregates in the sample, change in the signal/noise of the fluorescence intensity, or increase in A_{450} during the thermal denaturation experiments, which provided further evidence for the solubility of the constituents.

Thermal denaturation data were analyzed according to Pace et al. (*16*). Briefly, the equilibrium constant, *K*, was calculated for each temperature according to

$$K = (y_n - y)/(y - y_d) \quad (2)$$

where *y* is the measured tryptophan fluorescence intensity and y_n and y_d are the *y*-intercepts for the native and denatured forms of the protein, respectively. The free energy, ΔG, at each temperature was calculated by applying eq 3:

$$\Delta G = -RT \ln K \quad (3)$$

Values of the enthalpy (ΔH_m) and entropy (ΔS_m) at the midpoint as well as the thermal unfolding midpoint (T_m) were determined from a plot of ΔG versus *T*, because at the T_m, $\Delta G = 0$ and $\Delta H_m = (T_m)(\Delta S_m)$. The value of ΔH_m was confirmed by a van't Hoff plot, using eq 4:

$$\mathrm{d}(\ln K)/\mathrm{d}(1/T) = -\Delta H/R \quad (4)$$

Values for both the T_m and ΔH_m were also calculated by nonlinear least-squares analysis of the data using the thermal equivalent of eq 1, adapted from Eftink (*17*):

$$F_{\mathrm{Trp}} = \frac{[(y_n + m_n T) + (y_d + m_d T)\exp(-\Delta H_m/RT + \Delta H_m/T_m R)]}{1 + \exp(-\Delta H_m/RT + \Delta H_m/T_m R)} \quad (5)$$

The value of ΔG at room temperature, $\Delta G_{25\ ^\circ\mathrm{C}}$, was determined using the following:

$$\Delta G(T) = \Delta H_m(1 - T/T_m) - \Delta C_p[(T_m - T) + T\ln(T/T_m)] \quad (6)$$

where *T* is 298 K and ΔC_p represents the change in heat capacity associated with unfolding, calculated theoretically according to the method of Milardi (*18*).

Fibrillogenesis. The rV$_\lambda$6 proteins were dissolved in PBS at 1 mg/mL (the concentration was determined spectrophotometrically after filtration as described above); filtered PBS containing 10 μM thioflavin T (ThT) was heated to 37 °C in a 3 mL volume plastic cuvette. Immediately prior to data collection, an appropriate volume of protein solution was added to yield a final protein concentration of 35 μg/mL. ThT fluorescence intensity was measured using excitation and emission wavelengths of 450 and 490 nm with slit widths of 4 and 8 nm, respectively. The PMT voltage was set to 750 V. A micro-stir bar was used at 1 revolution per second to ensure adequate mixing of the solution. End-point solutions were used to test for the presence of fibrils using established techniques, i.e., Congo red staining and electron microscopy. Fibrillogenesis kinetics were analyzed by the following equation (*19*):

$$F_{\mathrm{ThT}} = A[\cosh(Bt) - 1] \quad (7)$$

where F_{ThT} is the fluorescence intensity of ThT, which serves as a measure of the amount of fibrils in solution, *A* is a factor

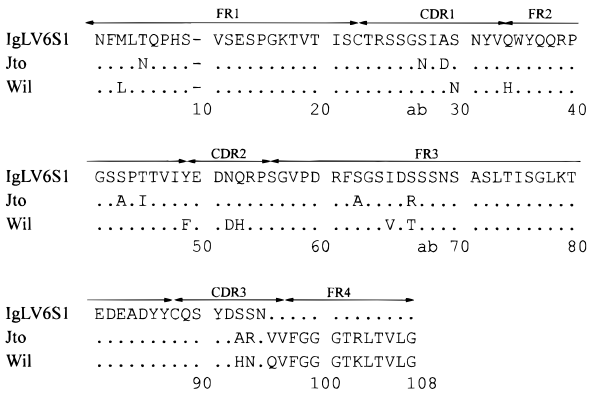

FIGURE 1: Comparison of the deduced amino acid sequences of rV$_\lambda$6Wil and -Jto with that of the V$_\lambda$6 germline gene. The framework (FR) and complementarity determining regions (CDR) are as indicated; the amino acid numbering system of Kabat (*33*) has been modified according to that used by Pokkuluri et al. (*20*).

related to the length of the lag phase, *B* is the effective rate constant, and *t* is the time in seconds. An absolute value of the lag time in seconds was calculated by extrapolating the linear region of the hyperbolic phase back to the abscissa.

RESULTS

The amino acid sequences of rV$_\lambda$6Wil and -Jto were 83% identical with respect to each other and approximately 90% to that encoded by the λ6 germline gene (Figure 1). Of note was the presence of Asp at position 29 in Jto, which changed the ionic character of CDR1. Other electrostatically significant replacements were the Arg residues at positions 68 and 94 that are located atop CDR loops 2 and 3, respectively [amino acid numbering according to Pokkuluri et al. (*20*)]. In addition, four electroneutral substitutions were unique to Jto: Asn5, Ile45, Ala63, and Ala93.

Bacterial expression of rV$_\lambda$6Jto yielded on average 10 mg of purified protein per 1.2 L of culture medium when the organisms were incubated at 37 °C. In contrast, expression of rV$_\lambda$6Wil under identical conditions as those used for rV$_\lambda$-6Jto resulted in accumulation of the protein in periplasmic inclusion bodies. Reduction in the incubation temperature to 30 °C and slowing the agitation speed increased substantially the concentration of soluble protein in the periplasmic space; however, the average yield of 2 mg per 1.2 L of culture medium was consistently less than that of rV$_\lambda$6Jto. When suspended in PBS solution, both rV$_\lambda$6Wil and -Jto were predominantly monomeric, exhibiting an apparent molecular mass of 11.5−12 kDa. Protein dimers contributed <10% of the total protein, calculated by integrating the area under the peaks, following curve-fitting analysis of the chromatography elution profiles (data not shown).

The thermodynamic stabilities of rV$_\lambda$6Wil and -Jto were quantified using both thermal and chaotropic denaturation methods. As noted previously, the denaturation of light chains appears to be a two-state, reversible process (*7*, *9*). The denaturation curves of rV$_\lambda$6Wil and -Jto induced by increasing concentrations of GdHCl were sigmoidal with a single asymptote, which supports a two-state unfolding model (Figure 2). The cooperativity-coefficient term, m_g (the gradient in the transition region), provided a measure of the internal stability of the protein with respect to the denaturation process. Values of −2.3 and −3.5 kcal/(mol·M) were

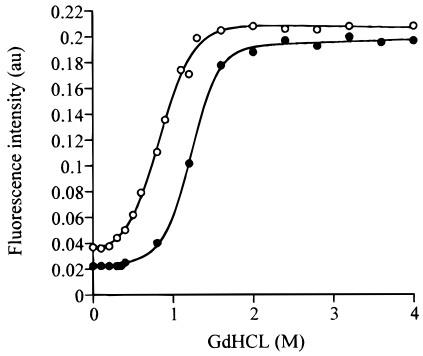

FIGURE 2: Determination of rV$_\lambda$6 protein stability by chaotropic denaturation. Proteins rV$_\lambda$6Wil and rJto were subjected to increasing concentrations of GdHCl in 10 mM sodium phosphate, pH 7.5. The fluorescence intensity of Trp35 in each sample was measured using excitation and emission wavelengths of 290 and 350 nm, respectively. Calculated values for the midpoint of the transition (C_m) were 0.83 and 1.22 M and for ΔG_{H2O} were 2.2 and 4.3 kcal/mol for rV$_\lambda$6Wil and rJto, respectively. Solid lines represent nonlinear, least-squares fits of the data using eq 1. (Reproduced with permission from "Amyloid and Amyloidosis 1998", Parthenon Publishing Group, NY.)

obtained for rV$_\lambda$6Wil and -Jto, respectively. The unfolding free energies (ΔG_{H2O}) of rVλ6Wil and -Jto were calculated to be 2.2 and 4.3 kcal/mol, respectively.

Thermal denaturation of the proteins in a PBS solution resulted in sigmoidal transitions for both rV$_\lambda$6Wil and -Jto (Figure 3A). The thermal unfolding midpoints (T_m) of rV$_\lambda$-6Wil and -Jto, calculated from plots of ΔG versus *T*, were 38.3 and 45.2 °C, respectively. Values of $\Delta G_{25\ °C}$ for both rV$_\lambda$6Wil and -Jto calculated using eq 5 (Figure 3A) are in agreement with those calculated indirectly according to Pace (*16*); all thermodynamic parameters are presented in Table 1. The van't Hoff analyses (eq 4, Figure 4) provided a direct measure of transition enthalpy, $\Delta H_{van't\ Hoff}$, that was in excellent agreement with ΔH_m calculated from the plot of ΔG versus *T*. Inclusion of 10 μM ThT in the solution had no effect upon the calculated values of the T_m (Figure 3B).

The fibrillogenesis of the rV$_\lambda$6 proteins shown in Figure 5 was monitored in real-time by measuring increases in the fluorescence intensity of ThT at 490 nm, which is considered indicative of fibril formation (*21*). Values of the lag time (t_{lag}) were calculated by extrapolating the linear region of the hyperbolic phase to the abscissa intersect, shown as the linear regression in Figures 6 and 7. The t_{lag} of rV$_\lambda$6Wil was 2380 s, which was significantly smaller than the calculated value of 21 800 s for rV$_\lambda$6Jto. Analysis of these data according to eq 7 resulted in quantitative parameters that describe the process of fibrillogenesis (*19*). The two parameters *A* and *B* represent the "shape" constant (related to the length of t_{lag}) and an effective rate constant, respectively. These variables were determined from the fibrillogenesis of both proteins by least-squares analysis (Table 2). The t_{lag} of rV$_\lambda$6Jto fibrillogenesis, 21 800 s, was approximately an order of magnitude longer than that of rV$_\lambda$6Wil; similarly, the rate constant, *B*, was approximately one-sixth that of rV$_\lambda$6Wil (Table 2).

Fibril formation was confirmed by ultrastructural analyses (Figure 8). Both V$_\lambda$6 proteins formed characteristic linear unbranching fibrils; however, fibrils composed of rV$_\lambda$6Jto appeared more rigid in structure compared to the shorter, twisted-ribbon appearance of the rV$_\lambda$6Wil fibrils.

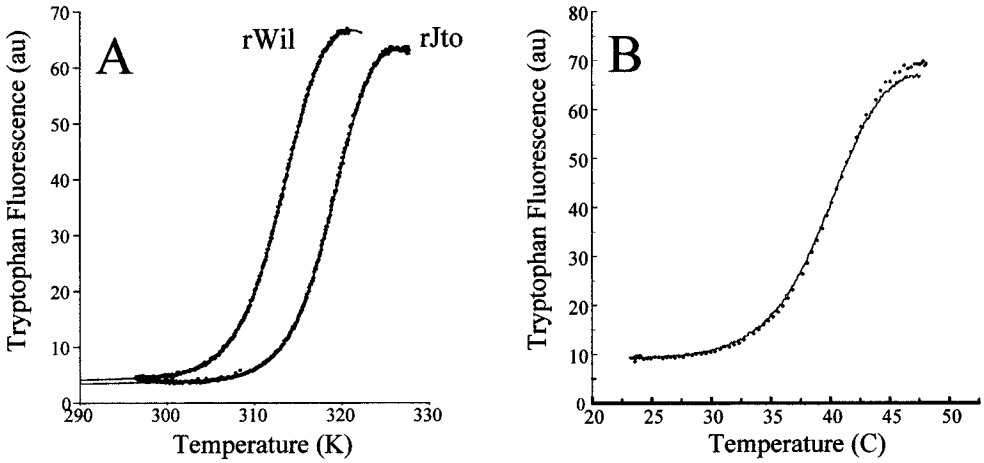

FIGURE 3: Determination of rV$_\lambda$6 protein stability by thermal denaturation. (A) Proteins rV$_\lambda$6Wil and rJto were suspended in PBS, pH 7.5, at 70 μg/mL; denaturation was induced by increasing the temperature from 25 to 55 °C in a single step. Solid lines represent the results of the curve-fitting analyses using eq 5. (B) Protein rV$_\lambda$6Wil in the presence and absence of 20 μM ThT. Calculated thermodynamic parameters are given in Table 1.

Table 1: Calculated Thermodynamic Parameters for rV$_\lambda$6 Wil and -Jto Determined by Chaotropic and Thermal Denaturation

parameter	Wil	Jto
T_m[a]	38.3 °C (311.6 K)	45.2 °C (318.5 K)
$\Delta G_{25\,°C}$[a]	3.0 kcal/mol	4.6 kcal/mol
$\Delta G_{25\,°C}$[b]	3 kcal/mol	4.1 kcal/mol
ΔG_{H2O}	2.2 ± 0.9 kcal/mol[e]	4.3 ± 1.0 kcal/mol
$\Delta H_m^{cDagger}$	80 kcal/mol	87 kcal/mol
$\Delta H_{van't\ Hoff}$[d]	80 ± 1.0 kcal/mol	87 ± 0.8 kcal/mol
ΔS_m	259 cal mol^{-1} deg^{-1}	275 kcal mol^{-1} deg^{-1}
C_m	0.83 ± 0.05 M GdHCl	1.22 ± 0.02 M GdHCl
m_g	−2.3 ± 0.9 kcal/(mol·M)	−3.5 ± 1.5 kcal/(mol·M)
ΔC_p	1.4 kcal/mol	1.5 kcal/mol

[a] Calculated according to Pace et al. (*16*) and using eq 6 with appropriate ΔC_p values. [b] Calculated from parameter values obtained using eq 5. [c] Calculated from a plot of ΔG vs T. [d] Calculated using eq 4. [e] Standard errors were calculated from least-squares analyses, with a 99% confidence limit.

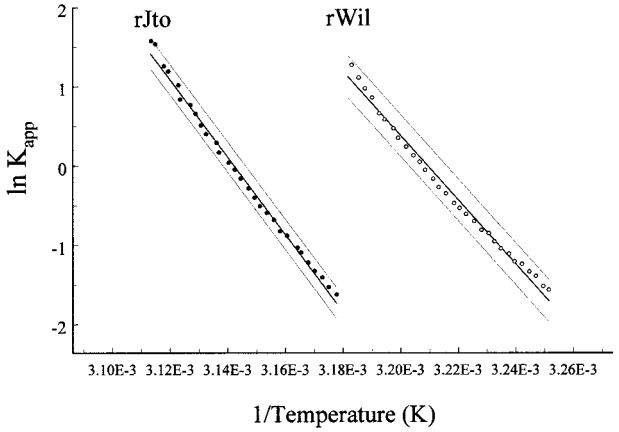

FIGURE 4: van't Hoff analysis of the thermal denaturation of rV$_\lambda$-6Wil and rJto. Data were obtained from the thermal denaturation of rV$_\lambda$6Wil and rJto in PBS, pH 7.5 (Figure 3A). Curves were analyzed using a least-squares fit to a linear equation; best fits are shown with 99% confidence limits. Calculated values of $\Delta H_{van't\ Hoff}$ are given in Table 1.

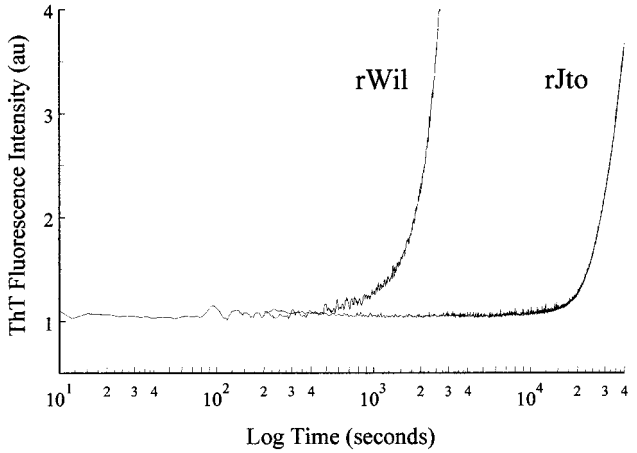

FIGURE 5: Fibrillogenesis of rV$_\lambda$6Wil and rJto. Proteins (35 μg/mL) were incubated in PBS, pH 7.5, at 37 °C in the presence of 10 μM ThT, and the fluorescence intensity was measured using excitation and emission wavelengths of 450 and 490 nm, respectively. (Reproduced with permission from "Amyloid and Amyloidosis 1998", Parthenon Publishing Group, NY.)

DISCUSSION

Fibrillogenesis and Thermodynamic Stability. Based upon comparative amino acid sequence data, it has been postulated that the presence of certain amino acid residues at particular positions within the V_L affect the propensity of light chains to form amyloid fibrils (*7*). It has been demonstrated experimentally that substitutions at these positions can effect V_L thermodynamic stability (*9*, *22*, *23*). It has been postulated that destabilizing substitutions result in a non-native aggregation-prone, pathologic form of the protein (*24*, *25*). This paradigm provides a theoretical framework for the analysis of light chain fibrillogenicity. Our studies have provided further evidence for a correlation between light chain thermodynamic stability and the propensity of these molecules to form amyloid.

The V_L amino acid sequence of Jto was highly similar to that of Wil and other amyloid-associated λ6 light chains; however, Jto was unique due to the presence at positions 29 and 68 of Asp and Arg, respectively. Although several amyloidogenic λ6 proteins accommodate either Asp29 (protein MAL2; unpublished results) or Arg68 [proteins K11, SUT (*26*), and THO (*27*)], both substitutions are unique to protein Jto. X-ray diffraction data have been obtained on crystals of rV$_\lambda$6Wil and -Jto (*20*); comparison of the three-dimensional structures revealed significant homology, with the exception in Jto of a salt-bridge between residues Asp29

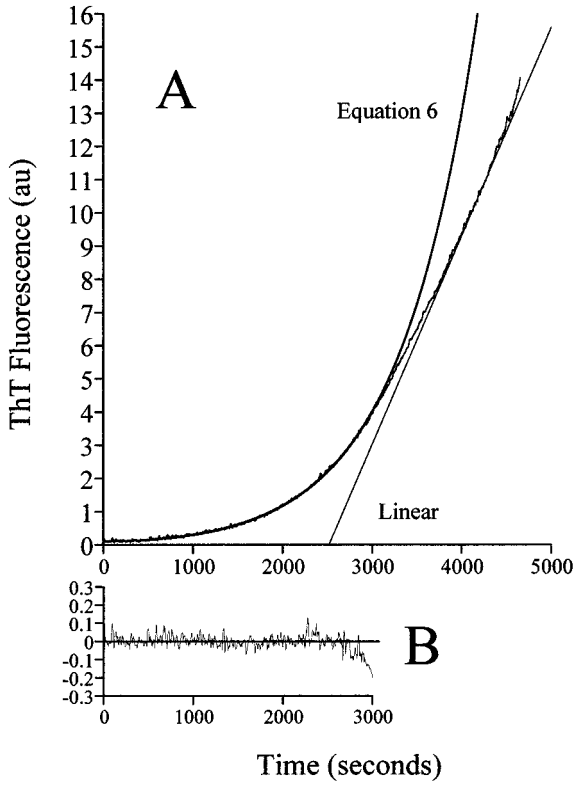

FIGURE 6: Analysis of rV$_\lambda$6Wil fibrillogenesis. The fibrillogenesis of rV$_\lambda$6Wil was monitored by measuring the ThT fluorescence intensity using excitation and emission wavelengths of 450 and 490 nm, respectively. Parameters *A* and *B* were determined by nonlinear least-squares fit using eq 7. The value of t_{lag} was determined by extrapolation of the linear region of the hyperbolic phase to the abscissa (linear). (B) Calculated residuals for the early phase (10%) of the analysis using eq 7. Values for *A* and *B* are given in Table 2.

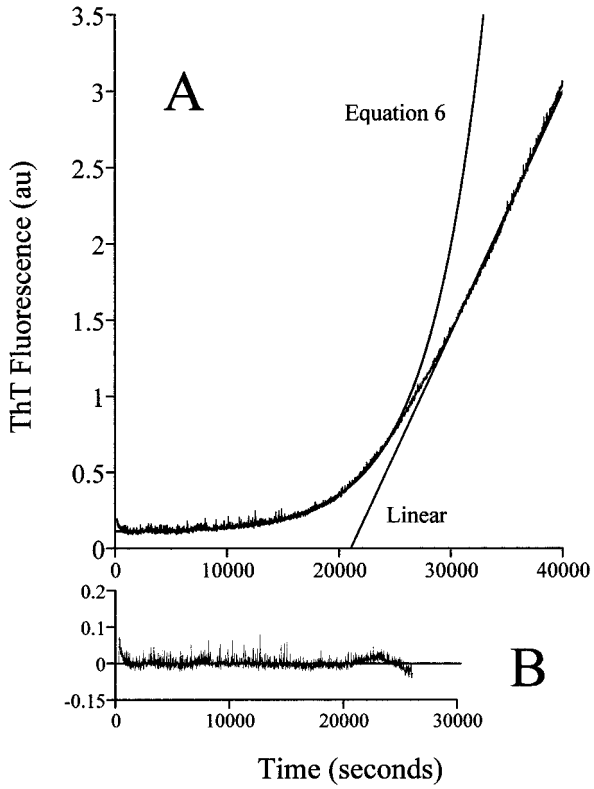

FIGURE 7: Analysis of rV$_\lambda$6Jto fibrillogenesis. The fibrillogenesis of rV$_\lambda$6Jto was monitored by measuring the ThT fluorescence intensity using excitation and emission wavelengths of 450 and 490 nm, respectively. Parameters *A* and *B* were determined by nonlinear least-squares fit using eq 7. The value of t_{lag} was determined by extrapolation of the linear region of the hyperbolic phase to the abscissa (linear). (B) Calculated residuals for the early phase (10%) of the analysis using eq 7. Values for *A* and *B* are given in Table 2.

and Arg68. We posit that this interaction contributed to the free energy of stabilization of Jto relative to Wil. The importance of salt bridge formation in stabilizing light chains has been described previously (*28*). The consequence of differences in the thermodynamic stability of the two proteins was evidenced during their bacterial expression. The formation of inclusion bodies by rV$_\lambda$6Wil at 37 °C is indicative of protein instability and has been previously correlated with destabilized mutants of the rV$_\kappa$4 protein REI (*23*). This observation implicates a temperature-dependent factor in determining the aggregation state of the Wil proteins.

Determination of the free energy of rV$_\lambda$6Jto and -Wil by thermal denaturation agreed with the value obtained by chaotropic denaturation; however, the ΔG_{H2O} was 0.8 kcal/mol lower than $\Delta G_{25\ °C}$, which may reflect the dependence of the $\Delta G_{25\ °C}$ calculation on ΔC_p. The assumption inherent to the van't Hoff analysis is that ΔH is temperature-independent. If, however, the heat capacity of the non-native protein differs from the native form, i.e., $C_p^{native} \neq C_p^{unfolded}$, ΔH will vary with temperature, and a nonlinear van't Hoff plot would result. This appeared to be the case for both λ6 proteins: rV$_\lambda$6Wil clearly exhibited a more substantial departure from linearity than rV$_\lambda$6Jto, as demonstrated by the increased width of the 99% confidence limit of the linear regression found for Wil as compared to Jto (Figure 4). In the absence of direct measurements of ΔC_p, values were estimated according to the theoretical method of Milardi (*18*) and ΔG was calculated by incorporating these values into eq 6. The error between ΔG_{H2O} and $\Delta G_{25\ °C}$ may reflect an underestimation of ΔC_p when calculating $\Delta G_{25\ °C}$.

Table 2: Calculated Kinetic Parameters for the Fibrillogenesis of rV$_\lambda$6 Proteins Wil and Jto

parameter	Wil	Jto
A	$(0.25 \pm 3.1) \times 10^{-3}$	$(6.65 \times 10^{-3}) \pm (1.2 \times 10^{-4})$
B (s^{-1})	$(1.22 \times 10^{-3}) \pm (0.5 \times 10^{-5})$	$(2.00 \times 10^{-4}) \pm (0.1 \times 10^{-5})$
t_{lag} (s^{-1})	2380	21800

The calculated ΔG_{H2O} values of both rV$_\lambda$6Wil and -Jto were considerably lower than reported values for the non-pathogenic V$_\kappa$4 LEN (9.7 kcal/mol) (*9*) and V$_\kappa$1 REI (6.8 kcal/mol) (*7*) proteins, but were similar in magnitude to that found for other unstable V$_L$ components (*7*). In addition, the C_m values of both rV$_\lambda$6 proteins were indicative of aggregation-prone V$_L$ proteins (*28*). The higher T_m of rV$_\lambda$6Jto was also indicative of increased thermal stability with respect to rWil. Previously, values ranging between 25 and 37 °C have been reported for aggregate-prone, recombinant mutants of the V$_\kappa$1 protein REI (*7*), temperatures which are significantly lower than the 55 °C T_m of the benign, wild-type REI (*29*) and another V$_\kappa$ protein, IVA (*30*). Both rV$_\lambda$6Wil and -Jto display ΔG, C_m, and T_m values characteristic of unstable proteins rather than the prototypic, nonpathologic light chains REI and LEN. If it is assumed a priori that the propensity to

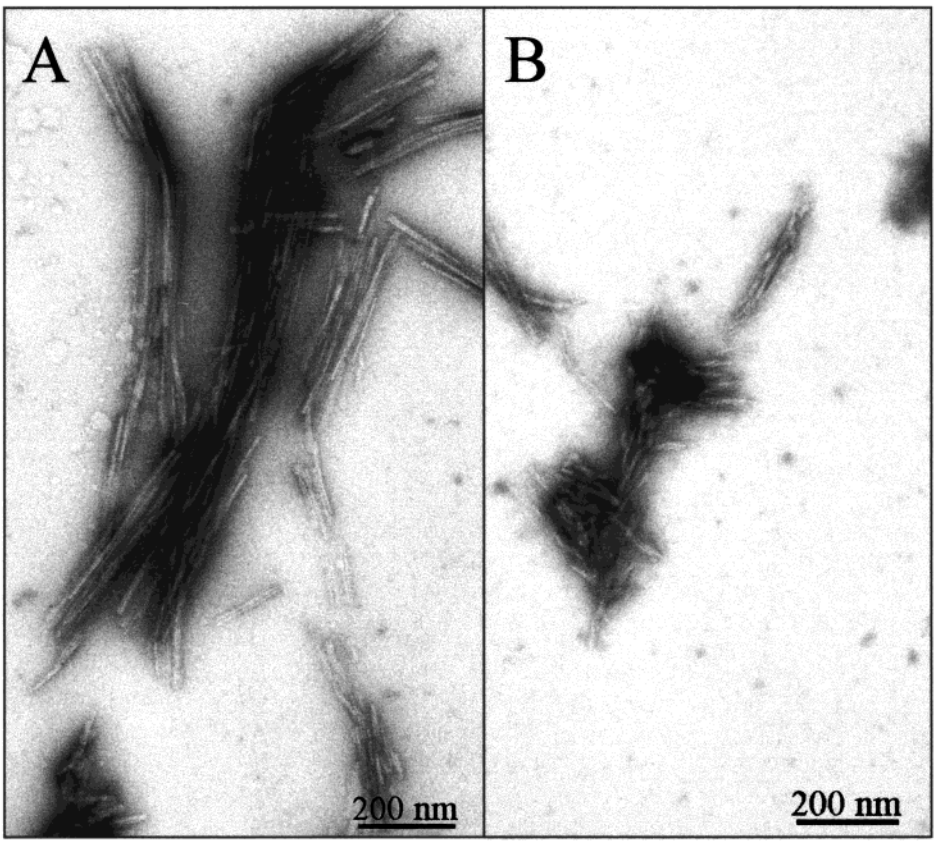

FIGURE 8: Ultrastructural analysis of fibrils formed by rV$_\lambda$6 proteins. Preparations of rV$_\lambda$6Jto (A) and -Wil (B) fibrils were dried on Formvar-coated copper grids and negatively stained using 4% uranyl acetate.

aggregate is related to protein stability, the thermodynamic data predict pathology associated with both rV$_\lambda$6Wil and -Jto. Although protein Jto did not form amyloid in vivo, this protein did deposit within renal tubules as amorphous casts.

Thermal denaturation experiments were performed using both proteins in the presence of ThT at the concentration used in the fibril-forming assays. A previous study has demonstrated that the amyloidophilic dye Congo red had the ability to preferentially interact with, and stabilize, non-native conformations of light chains (*31*). Inclusion of ThT in the reaction mixture, however, established that the dye did not stabilize a non-native form of the protein, which would have been manifest as an inflection in the denaturation curve.

Despite protein Jto being deposited in vivo as amorphous renal tubular casts and protein Wil as AL fibrils, both rV$_\lambda$6 components formed fibrils in vitro under similar conditions (Figures 5−8). However, there was a considerable difference between the two components in the rate of fibril formation. Fibrillogenesis kinetics are characterized by a lag time (t_{lag}) followed by a period of rapid polymerization. Kinetic analyses of the initial 10% of the polymerization reaction (Figures 6 and 7) were in excellent agreement with the double-nucleation theory of Bishop and Ferrone (*19*) as confirmed by the small χ^2 values of 0.15 and 0.04 for rV$_\lambda$-6Wil and -Jto, respectively. The model describes a process in which fibrillogenesis is initiated by homogeneous nucleation, which is rate limiting, followed by the addition of monomers to the growing fibril. Subsequently, the de novo formation of seeds is not a prerequisite in the propagation of new fibrils: fragmentation, heterogeneous nucleation, and lateral growth may all contribute to secondary nucleation events. The precise nature of the secondary nucleation process in the fibrillogenesis of V$_\lambda$6 proteins is under investigation. The fibrillogenesis kinetics of rV$_\lambda$6Wil and rV$_\lambda$-6Jto clearly demonstrated that both proteins form fibrils in this system; however, there were clearly distinguishing differences: the most outstanding being the length of t_{lag}. It is assumed that the shorter the lag time the more prone the protein is to initiate fibril formation. The lag phase of rV$_\lambda$-6Wil was an order of magnitude less than that of rV$_\lambda$6Jto; similarly, the rate constant associated with rV$_\lambda$6Wil fibrillogenesis was 6 times faster than that for rV$_\lambda$6Jto. Catabolic clearance of free light chains from the circulation occurs within approximately 3.6 h (*32*). The fibrillogenesis of rV$_\lambda$-6Wil is rapid with respect to the rate of catabolism. In contrast, based upon the length of t_{lag}, it is anticipated that catabolic clearance would effectively compete with, and prevent, Jto from forming amyloid. In addition, the aggregation rate of Jto in vivo, resulting in tubular cast deposits and renal failure, may also have prohibited amyloidogenesis by sequestration of the monomer at a rate faster than that of homogeneous nucleation.

Fibrillogenesis and the Non-Native State. At 37 °C, a substantial population of rV$_\lambda$6Wil is present in a non-native state, approximately 35%, calculated from the thermal denaturation curve (Figure 3) and assuming a two-state transition. Conversely, the value for rJto is only 5%. During expression of rV$_\lambda$6Wil in *E. coli* at 37 °C, the majority of the protein was present as insoluble aggregates in periplasmic inclusion bodies. However, when the temperature was reduced to 30 °C, at which only 5% of rV$_\lambda$6Wil is non-native, the protein was readily extracted in a soluble form, akin to

rV$_\lambda$6Jto at 37 °C. Expression of destabilized rV$_\kappa$ mutants also resulted in inclusion body formation (*23*). Thus, it is posited that due to its thermodynamic instability, the potential for rV$_\lambda$6Wil fibrillogenesis was greater at 37 °C, due to an increase in the population of protein in a non-native, amyloidogenic state. In contrast, the more thermostable rV$_\lambda$-6Jto had a greater thermodynamic stability and was considerably less fibrillogenic at 37 °C, which is coincident with a small non-native population. We attribute the absence of detectable amyloid deposits in patient Jto to this enhanced stability. Thus, the fibrillogenic potential of the two V$_\lambda$6 proteins correlated with their thermodynamic instability, but perhaps, more importantly, it was directly related to the size of the non-native rV$_\lambda$6 population. These data support the hypothesis that fibrillogenesis arises from proteins which adopt a non-native, aggregate-prone configuration. These studies also provide evidence for the physiological relevance of our fibrillogenesis assay. The ability to determine readily the thermodynamic stability of Bence Jones proteins has prognostic value in differentiating amyloid from nonamyloidogenic light chains. Additionally, the fact that this assay can also be used to test compounds that can inhibit AL fibril formation has therapeutic import for patients with this invariably fatal disease.

ACKNOWLEDGMENT

We are indebted to Prof. Ron Wetzel for invaluable discussions and Dr. John Dunlap, who performed the electron microscopy work. Dr. Mitch Klebig assisted in the preparation of the recombinant proteins.

REFERENCES

1. Falk, R. H., Comenzo, R. L., and Skinner, M. (1997) *N. Engl. J. Med. 337*, 898−909.
2. Westermark, P. (1997) *Amyloid: Int. J. Exp. Clin. Invest. 4*, 216−218.
3. Harper, J. D., and Lansbury, P. T. (1997) *Annu. Rev. Biochem. 66*, 385−407.
4. Isobe, T., and Osserman, E. F. (1971) *N. Engl. J. Med. 290*, 473−477.
5. Pascali, E. (1995) *Crit. Rev. Oncol. Hematol. 19*, 149−181.
6. Solomon, A., Weiss, D. T., and Kattine, A. A. (1991) *N. Engl. J. Med. 324*, 1845−1851.
7. Hurle, M. R., Helms, L. R., Li, L., Chan, W., and Wetzel, R. (1994) *Proc. Natl. Acad. Sci. U.S.A. 91*, 5446−5450.
8. Bellotti, V., Stoppini, M., Mangione, P. P., Fornasieri, A., Min, L., Merlini, G., and Ferri, G. (1996) *Biochim. Biophys. Acta 1317*, 161−167.
9. Stevens, P. W., Raffen, R., Hanson, D. K., Deng, Y.-L., Berrios-Hammond, M., Westholm, F. A., Murphy, C., Eulitz, M., Wetzel, R., Schiffer, M., and Stevens, F. J. (1995) *Protein Sci. 4*, 421−432.
10. Abe, M., Ozaki, S., Wolfenbarger, D., deBram-Hart, M., Weiss, D. T., and Solomon, A. (1994) *J. Clin. Lab. Anal. 8*, 4−9.
11. Chirgin, J. M., Przybyla, A. E., MacDonald, R. J., and Rutter, W. J. (1979) *Biochemistry 18*, 5294−5299.
12. Ch'ang, L.-Y., Yen, C.-P., Besl, L., Schell, M., and Solomon, A. (1994) *Mol. Immunol. 31*, 531−536.
13. Sanger, F., Nicklen, S., and Coulson, A. R. (1977) *Proc. Natl. Acad. Sci. U.S.A. 74*, 5463−5467.
14. Sambrook, J., Fritsch, E. F., and Maniatis, T. (1989) *Molecular Cloning: A Laboratory Manual*, 2nd ed., Cold Spring Harbor Laboratory Press, Cold Spring Harbor, NY.
15. Santoro, M. M., and Bolen, D. W. (1988) *Biochemistry 27*, 8063−8068.
16. Pace, C. N., Shirley, B. A., and Thomson, J. A. (1989) in *Protein Structure: a Practical Approach* (Creighton, T. E., Ed.) pp 311−330, IRL Press, Oxford.
17. Eftink, M. R. (1995) *Methods Enzymol. 259*, 487−512.
18. Milardi, D., la Rosa, C., Fasone, S., and Grasso, D. (1997) *Biophys. Chem. 69*, 43−51.
19. Bishop, M. F., and Ferrone, F. A. (1984) *Biophys. J. 46*, 631−644.
20. Pokkuluri, P. R., Solomon, A., Weiss, D. T., Stevens, F. J., and Schiffer, M. (1999) *Amyloid: Int. J. Exp. Clin. Invest.* (submitted for publication).
21. Naiki, H., Higuchi, K., Hosokawa, M., and Takeda, T. (1989) *Anal. Biochem. 177*, 244−249.
22. Hurle, M. R., Helms, L. R., Li, L., Chan, W., and Wetzel, R. (1994) *Proc. Natl. Acad. Sci. U.S.A. 91*, 5446−5450.
23. Chan, W., Helms, L. R., Brooks, I., Lee, G., Ngola, S., McNulty, D., Maleeff, B., Hensley, P., and Wetzel, R. (1996) *Folding Des. 1*, 77−89.
24. Helms, L. R., and Wetzel, R. (1996) *J. Mol. Biol. 257*, 77−86.
25. Kelly, J. W. (1996) *Curr. Opin. Struct. Biol. 6*, 11−7.
26. Solomon, A., Frangione, B., and Franklin, E. C. (1982) *J. Clin. Invest. 70*, 453−460.
27. Ghiso, J., Solomon, A., and Frangione, B. (1986) *J. Immunol. 136*, 716−719.
28. Wetzel, R. (1997) *Adv. Protein Chem. 50*, 183−242.
29. Helms, L. R., and Wetzel, R. (1995) *Protein Sci. 4*, 2073−2081.
30. Zav'yalov, V. P., Troitsky, G. V., Khechinashvili, N. N., and Privalov, P. L. (1977) *Biochim. Biophys. Acta 492*, 102−111.
31. Piekarska, B., Skowronek, M., Rybarska, J., Stopa, B., Roterman, I., and Konieczny, L. (1996) *Biochimie 78*, 183−189.
32. Solomon, A., Waldmann, T. A., Fahey, J. L., and McFarlane, A. S. (1964) *J. Clin. Invest. 43*, 103−117.
33. Kabat, E. A., Wu, T. T., Perry, H. M., Gottesman, K. S., and Foeller, C. (1991) *Sequences of proteins of Immunological Interest*, Vol. 5th, National Institutes of Health, Bethesda, MD.

BI991131J